ELECTROCHEMICAL PROPERTIES OF LITHIUM ION CONDUCTING SOLID POLYMER ELECTROLYTES

M. Watanabe, C. S. Velázquez, Zeev Porat, Otto Haas, T. T. Wooster, M. L. Longmire, H. Zhang, H. Nishihara and Royce W. Murray*

Kenan Laboratories of Chemistry, Univ. of No. Car., Chapel Hill, NC 27599-3290

In 1985 our laboratory initiated an investigation of the electrochemical reactions of molecular electron donor/acceptor species dissolved in solid and semi-solid solvents. Poly-ether polymer electrolytes were selected as the model solid and semi-solid solvents, and the redox species have included ferrocenes[1,2], metal bipyridine complexes[3], tetracyanoquinodimethane[4] (TCNQ), and derivatives[5,6] in which poly-ether chains have been attached to such species. The thrust of this investigation was firstly, to develop methodology for obtaining quantitatively interpretable electron transfer and mass transport rates of such molecular solutes in solid or semi-solid solvents, and secondly, to explore ways in which their solid state behavior differs from that familiar in fluid electrolyte solutions. This paper will draw together the essential aspects of the microelectrode-based[7] solid state voltammetry methodology developed, and describe some of the special aspects of electron transfer and mass transport dynamics observed during this still on-going investigation.

Methodology For Solid State Voltammetry Of Electron Carriers Dissolved in Poly-Ether Polymer Electrolytes

The central experimental issue in solid state voltammetry in polymer solvents is that all mass transport phenomena, microscopic and macroscopic, are much slower than in fluid solutions based on monomeric solvents. The underlying control of slow transport through a polymer matrix lies in the rates of successive microscopic displacements of segments of the polymer chains that comprise the solvent. The specific dynamics of polymer chain segmental motions depend on the polymer structure and on any interactions between the polymer chains and the solutes.

In a polymer electrolyte[8] consisting of a poly-ether solvent, a dissolved salt such as $LiClO_4$, and a molecular electron donor/acceptor couple, the mobility of both electrolyte ions and

D/A solute can be very small. The room temperature ionic conductivity of even a concentrated solution of $LiClO_4$ (say, one mole of $LiClO_4$ per 16 ether oxygens, e.g., O/Li = 16, which is ca. 1.7 M) may be 10^{-4} S cm^{-1} in a "good" case, and usually is orders of magnitude smaller. A typical room temperature diffusivity of a D/A solute in a poly-ether is ca. 10^{-8} cm^2/s, but it can be much smaller, by as much as 10^7-fold. These facts dominate the design of voltammetric experiments in poly-ether polymer electrolytes.

Consider first the problem of low ionic conductivity. If the product iR_{unc} of current resulting from an electrode reaction of a D/A solute couple and the uncompensated (by the three electrode potentiostat) solution resistance is a significant portion of the applied potential, effective control of potential applied to the interface to drive the D/A electrode reaction is lost. We have employed a strategy successful in other ionically resistive low dielectric monomer solvents like benzene and heptane[9], namely the use of microelectrodes, which cause iR_{unc} to be small by allowing the currents to be small. This tactic has been generally effective.

Microelectrode currents for D/A reactions depend on the D/A concentrations as well as on diffusion coefficients D_{app}, and when both are small the currents can become so small that their measurement is difficult. Currents down to ca. 1 pA can be measured using suitable potentiostat electronics and shielding; lower currents provoke interest in increasing the D/A concentration, which depends on the D/A solubility in the polymer. Here one discovers that numerous interesting D/A species have limited solubility in poly-ethers. One solution to this measurement problem is to synthetically attach poly-ether tails to the D/A species[5,6] to make them more compatible with the poly-ether solvent environment. Another solution is to make use of microband rather than microdisk electrodes. Microbands are more difficult to fabricate, but offer advantages of larger currents without commensurate penalty from iR_{unc} effects.

Table I presents relations[7,10] for currents and uncompensated resistances at microdisk and microband electrodes. The current relations fall into two categories, so-called radial and linear diffusion. Diffusion is linear when diffusional pathlengths are small in comparison to the microdisk electrode radius (or in the case of the microband, the width of the microband). The pertinent equation for peak current in potential sweep voltammetry is the classical Randles-Sevcik Equation[11] (1) and (3), which differs for microdisk and microband only in the statement of electrode area. We frequently observe linear diffusion conditions, even with microelectrodes, in

polymer electrolytes because the diffusion coefficient values are so small. Diffusional pathlength is given by the relation $[2Dt]^{1/2}$ where t is the measurement timescale which in voltammetry is long or short according to the rate of potential sweep. Radial diffusion ensues when $[2Dt]^{1/2}$ is comparable to or larger than the electrode radius; this occurs infrequently in polymer electrolyte solutions. Radial diffusion currents are steady state at microdisks (Eqn. (2)) and at microbands decay weakly with time (Eqn. (4)).

Examination of the relations in Table I reveals several important aspects of resistive medium measurements and of microband vs. microdisk properties. The equations show that microband currents are much larger than microdisk currents (Eqns. (5), (6)) since band length L typically greatly exceeds the microdisk radius r. The uncompensated resistance losses iR_{unc} at these electrodes (the products of the disk or band currents and respective resistance relations), are in the case of radial diffusion (Eqns. (14), (16)) independent (microdisk) or nearly independent (microband) of the electrode size. For linear diffusion, the uncompensated resistance loss iR_{unc} (Eqns. (13), (15)) is for microdisks and microbands proportional to radius and width, respectively, so that smaller dimensions will allow improved voltammetric potential control for both disks and bands. The ratio of uncompensated resistance loss for a microdisk to that for a microband (Eqns. (17), (18)) is for both diffusions near unity since the dimensions of r and w are commonly similar.

The important conclusions drawn from these comparisons are that, under linear diffusion conditions, iR_{unc} effects are always ameliorated by use of smaller electrodes, and under either linear or radial conditions, larger currents are obtained from microbands but the larger currents are not accompanied by commensurate increase in iR_{unc}. Accordingly, microbands are a powerful tool to employ when one seeks larger currents because of limited solubility or slow diffusion of the D/A species.

Figure 1 shows examples of potential sweep voltammetry that illustrate waveshapes obtained under radial and linear diffusion conditions. Figure 1A is a nearly steady state, radial diffusion example[12] for a ferrocene poly-ether derivative dissolved in a poly-ether electrolyte of MW 20,000. The radial diffusion condition was promoted in this case by use of a very slow potential sweep rate and an elevated temperature. The value of D_{app} calculated from the radial Eqn. (2), 1.1×10^{-8} cm^2/s, was confirmed by a potential step chronoamperometric experiment that

under linear diffusion conditions gave D = 0.98×10^{-8} cm^2/s. Figure 1B contrasts the linear and radial diffusion-controlled oxidation and reduction waves that are observed[4] at 23°C and 101° C, respectively, for the radical anion of $TCNQ^-$ dissolved in a network poly-ethylene oxide[8f]. The radial diffusion condition was promoted by the faster diffusion at the elevated temperature. The oxidation currents are larger than the reduction currents. This difference becomes larger at higher concentrations of $TCNQ^-$ as discussed later. Figure 1C, the oxidation of ferrocence sites in an undiluted molecular melt, illustrates[5] an all-to-frequent observation in polymer electrolyte voltammetry, a diffusion condition intermediate between linear and radial diffusion. To unravel the diffusion constant in such cases, we generally resort to potential step chronoamperometry, for which the necessary appropriate mathematics are somewhat simpler. We apply chronoamperometry to linear diffusion cases as well, as a cross-check on the potential sweep voltammetry result.

The numerous other aspects of experimentation in poly-ether solutions have been recently discussed[14].

Donor/acceptor Diffusion Rate Measurements In Polymer Electrolytes

Understanding ionic conductivities of salts dissolved in poly-ethers and related polymer solvents has been an interesting and actively investigated topic over the roughly 15 years since Armand's initial report of the polymer electrolyte characteristic galvanized research by numerous groups[8]. It is now appreciated that the mobility of the dissociated salt's ions must be unfolded from its ion pairing and higher multiplet association phenomena, which is a substantial complication. Understanding ionic conductivity additionally involves the metal-ether coordinative thermodynamics and kinetic lability, which in the first instance dissolves the metal salt but in the second makes the cation less mobile than the anion and restricts the segmental mobility of the poly-ether chains. That is, the very coordination that generates the polymer electrolyte tends to immobilize the cation on the poly-ether matrix, causing a transference number difference $t_+ < t_-$ and slowing the chain motions upon which transport of the ions and of any other solute within the polymer phase depends. One result of these effects is that while ionic conductivity of lithium salts increases at low electrolyte concentrations, it often maximizes and then decreases at higher concentrations.

Molecular transport in polymer electrolytes is in some respects simpler than ionic

conductivity. Since the transported species is an electron not just an ionic charge carrier, and moves under a concentration gradient, ion-pairing has a minor importance in transport rates. That is, D_{app} is in principle unrelated to the D/A ionic charge. Ionic conductivity, in contrast occurs through electrical potential gradients and depends on ionic charge as well as mobility. Further, observing D/A electrochemical reactions requires attaining an adequate level of ionic conductivity with a supporting electrolyte, which can be the same lithium salts that are of intrinsic ionic conductivity interest. Accordingly the D/A transport usefully occurs in a matrix germane to the ionic conductivity problem.

Molecular D/A transport additionally entails its own interesting complexities in a wide range of specific chemistry of the diffusant, i.e., its molecular size, degree of association with the poly-ether matrix, and electron transfer dynamics. The latter refers to the coupling of physical transport with electron self exchange reactions in the electrode depletion layer, which has no counterpart in ionic conductivity phenomena.

Molecular transport rates will be discussed using selected but typical (Table II) diffusion constants that we have measured using microelectrode voltammetry as discussed above. The data are chosen to illustrate various significant transport dependencies.

Effects of Electron Donor/Acceptor Molecular Dize and Concentration.

Table I contains several examples of varied the D/A molecular size. Entries #1-4 were studied in network PEO where it was also found (for Entry #3 as an example) that the use of higher concentrations of the ferrocene redox species depressed the measured diffusion coefficient. The latter behavior is formally similar to that of the ionic conductivity of $LiClO_4$ at concentrations high enough that conductivity decreases with increasing $LiClO_4$ concentration. The decrease in ionic conductivity at increased $LiClO_4$ is attributed to depression of the polymer segmental dynamics by coordinative, transient cross-linking interactions of ether sites with the increasing population of Li^+ ions. The parallel ferrocene behavior suggests that these solutes can also be regarded as appreciably interacting with the poly-ether matrix, as opposed to solutes that provoke the opposite effect (e.g., diffusion-plasticization, where transport rates increase with concentration), as considered below. The diffusion constant for Entry #4 is the smallest with this series, even though this hydrophobic species should exert the weakest interaction with the poly-ether. Entry #13 is similarly hydrophobic and bulky, with a similarly smaller D value than

Entries #1-3. This is taken to imply that increased chain segmental displacement requirements imposed by a diffusant size can be of larger consequence than interaction effects on the diffusion rate. Note concurrently that it is not straightforward to separate the consequences of solute/polymer interactions from those of diffusant molecular size.

Entries #9 and 10 provide a clearer comparison of diffusant size, comparing transport of ferrocene carboxylic acid with that of the same molecule but amidized with a methyl-end-capped poly-ether chain of the same MW as the methyl-end-capped MPEG-2000 poly-ethylene oxide solvent. Diffusion of the latter ferrocene is more than 10-fold slower[5] than that of the monomeric $CpFeCO_2H$ solute. In this example of the effect of molecular size on diffusion rate, the D_{app} of the FcMPEG derivative appears to measure mainly the self-diffusivity of the poly-ether tail, as opposed to that of the ferrocene head. The poly-ether is expected to diffuse as a random coil since the molecular weight used is lower than the critical entanglement value for poly-ethylene oxide. A related point is whether the slower diffusion of FcMPEG might in part be caused by the strong interaction of the Li^+ cation with its poly-ether tail, an effect absent in the transport of the $CpFeCpCO_2H$ solute. More recent measurements[12] have shown that this interaction has a modest effect on the diffusion of poly-ether-tailed ferrocenes at O/Li ratios as small as 16, but no effect at all in a more dilute electrolyte where O/Li = 250.

Effects of Electrolyte Concentration.

Increasing electrolyte concentration has a dramatic effect on molecular D/A diffusivity as illustrated by Entries #19-26 for the $TCNQ^{1-/2-}$ data. A five-fold increase in electrolyte concentration causes a ca. 10^2-fold drop in the $TCNQ^-$ diffusion rate. This change is unrelated to electrolyte-induced polymer crystallinity; the cross-linked network PEO phase is isotropic through this range of conditions. The effect of increasing Li^+ concentration is readily understood as reflecting chain segmental dynamics depressed by enhanced Li^+ coordinative binding to and cross-linking of the poly-ether chains.

The electrolyte concentration effect can be fairly reliably invoked to manipulate D/A solute diffusivity to investigate circumstances of extremely slow diffusion, when that is desired. For example, we have in recent work[15] employed a 1:1 mole addition of $LiClO_4$ electrolyte to depress self-diffusivity in a cobalt bipyridine complex-poly-ether derivative molecular melt by ca. 10-fold to a value as low as $7x10^{-16}$ cm^2/s. Also, one can resort to other oxygen-loving metal

ions such as Mg^{2+} to depress solute transport rates. These tactics of course also depress ionic conductivity, which must be taken into account when designing the voltammetric measurements.

Effects of Polymer Phase-State and Diffusion-Plasticization.

Measurements of the temperature dependency of the diffusivity of $CpFeCpCO_2H$ and of FcMPEG dissolved in MPEG-2000, Entries #9-12, are illustrated in Figure 2. Differential scanning calorimetry of the poly-ether host, MPEG-2000, shows that it exhibits a melting transition at 54°C; both the molecular diffusion rates in Figure 2 exhibit a sharp drop starting at about 52°C. At higher temperatures, diffusion occurs in an isotropic polymer melt. The sharp drop in diffusivity below 52°C is driven by an onset of partial crystallinity of the polymer electrolyte matrix. The details of this drop in diffusion rate are not well understood; transport in any randomly non-isotropic matrix is a complex topic.

Figure 2 additionally shows that the difference in diffusion rate of the monomeric $CpFeCpCO_2H$ and the poly-ether tailed FcMPEG persists throughout a very wide range of diffusion values that span the isotropic melt and the partially crystalline state.

Another example of the effect of poly-ether phase-state is shown by entries #5 vs. 7 and #6 vs. 8. Here measurements of D_{app} were made by casting a film of mixed valent ferrocene poly-ether solution onto an interdigitated electrode array. Application of a bias potential between the finger-sets of the IDA produces a steady state concentration gradient in the gap between fingers, with limiting currents from which D_{app} is straightforwardly obtained. The short-chain poly-ether MPEG-400 (MW=400) is a melt at room temperature whereas the longer MPEG-1000 (MW=1000) is a soft (partly crystalline) wax. This mild degree of partial crystallinity provokes a 10-fold depression in D_{app}. Note additionally that the higher concentration of ferrocene in each poly-ether has a smaller D_{app} analogous to results in network PEO discussed above.

The experiments with $[Os(phen)_3]^{2+}$ diffusing in a high MW linear PEO (Entries #16-18) give an additional phase-state example, as well as one of "diffusion-plasticization". The diffusivity of $[Os(phen)_3]^{2+}$ is readily measured at 65° C, above the polymer solvent's melting transition, but diffusion was too slow and ionic resistivity too large for a successful measurement in dry poly-ether at room temperature. Bathing the film of polymer electrolyte in acetonitrile vapor, on the other hand, elevates $[Os(phen)_3]^{2+}$ diffusivity and $LiCF_3SO_3$ ionic conductivity to measurable levels, even for small sorbed quantities of CH_3CN. This diffusion-plasticization is

interpreted as reflecting coordinative competition of the sorbed CH_3CN for Li^+ions, breaking (or lessening) the Li^+-induced cross-linking of the polymer chains. In more general terms, the specific chemical nature of the sorbed CH_3CN causes an action to reduce polymer chain interactions and polymer-solute interactions, enhancing segmental chain dynamics and mobility of ions and diffusant. A number of other small organic molecules sorbed at vapor/polymer boundaries act in a similar manner. Diffusion-plasticization is a convenient tool for enhancing diffusivities that are too small to be conveniently measured, but its quantitative reproducibility requires careful control of the bathing vapor-polymer film equilibrium.

Electron Transfer Coupling With Physical Diffusion.

Reduction or oxidation of a diffusing solute to a stable, diffusing redox partner causes the depletion layer around the electrode to be a mixed valent D/A solution, within which electron self-exchange reactions between the donor and acceptor couples can occur. Such processes have negligible importance in fluid electrolyte solutions, but for redox couples with large self-exchange rate constants k_{ex} become important when the rate of physical diffusion is slow. The pertinent comparison, of the time constant $\tau_{diff} = \delta^2/D_{phys}$ for the D/A pair to physically diffuse towards one another over a distance δ, with the time constant $\tau_{et,\delta} = 1/k_\delta C$ for exchange of an electron between D and A over the same distance, is embodied in the Dahms-Ruff relation[16,17] which expresses the enhanced, or apparent diffusion D_{app} of the electron or hole carrier D or as the summation

$$D_{app} = D_{phys} + \frac{k_\delta \delta^2 C}{6} \tag{19}$$

where k_δ is the electron self exchange rate constant at distance δ and C is donor plus acceptor concentration.

Equation (19) predicts a linear plot of D_{app} against C, provided D_{phys} is independent of concentration. The preceding discussion shows however that diffusion rates in polymer solvents often vary with concentration. In a study of diffusion within solvent-wetted polymer films on chemically modified electrodes, Anson and Buttry demonstrated[18] the virtue of using a redox diffusant ($[Co(bpy)_3]^{2+}$) which can be both oxidized and reduced, and where one of the two D/A pairs has a small electron self-exchange constant (and thus measured D_{phys}) and the other a large one in which the electron exchange would enhance diffusion as described by Equation (19).

Table II Entries #19-26 are data from a study[4] of diffusion-electron transfer coupling in

the $TCNQ^{-/0}$ couple. Figure 1B above illustrated the difference in apparent diffusivities of $TCNQ^-$ when it is oxidized vs. being reduced; the difference increases at higher $TCNQ^-$ concentration. The reduction couple, $TCNQ^{-/2-}$, is taken as measuring D_{phys} and the oxidation couple $TCNQ^{-/0}$ as reflecting an electron exchange-enhanced diffusion. Plots of the difference $[D_{app}-D_{phys}]$ vs. C are linear as expected from Equation (19); values of $k_\delta\delta^2$ obtained from the slopes of such plots are given in the Table.

Prior to obtaining these $k_\delta\delta^2$ data for $TCNQ^{-/0}$ (those in the Table are only a small sample of the data collected[4]), it had been assumed in a number of related applications of the Dahms-Ruff equation that (a) the electron transfers between D and A would occur at collision-contact (e.g., δ is twice the D/A radius) and (b) if D_{phys} were very small the rate of electron transfer could become limited by the occurrence rate of collisions (e.g., Smolokowski-limited). The $TCNQ^{-/0}$ results led us to the realization[4] that assumption (a) could not be taken generally, and that assumption (b) was an incorrect conclusion in the original theory papers.[16] In the cubic lattice model on which Equation (19) is based, the collision rate is actually already accounted for in the form of the D_{phys} term.

Examination of Equation (19) in that light suggests that if the value of D_{phys} is sufficiently small, that of D_{app} should reach a minimum limiting value. The Entry #19-26 data in Table II show that this does not occur; $k_\delta\delta^2$ continues to decrease as D_{phys} decreases. In fact, a plot of a large collection of $k_\delta\delta^2$ data against the corresponding D_{phys} values shows[4] a linear correlation over nearly a 10^5-fold range of values. That electron transfer does not require collision-contact is the key to understanding this correlation; i.e., as D_{phys} decreases, electron transfers occur at progressively longer distances, but with progressively slower rate constants according to the well-known relation[19]

$$k_g = k_\Delta e^{-\beta r} \qquad (20)$$

where k_Δ represents the contact electron self exchange rate constant (center-to-center contact distance Δ), r is edge-to-edge separation at electron transfer (i.e., $\Delta + r = \delta$), and β is a electronic coupling constant. This exponential reaction rate-reactant distance relation means that electron transfers always favor short distances when the reactants are physically very mobile, but when

the reaction partners approach one another very slowly, the rate of electron delivery at a larger reactant separation (even though $k_\delta < k_\Delta$) can compete with the slow rate of the D/A diffusional approach. The electron transfer and diffusive processes can thereby remain in a competitive balance over a wide range of D_{phys}. The distances (r) of electron transfer estimated[4] for the $TCNQ^{-/0}$ data in Table II range from 3 to 16Å. While the long distance electron transfer process is of intrinsic interest, the variability of the electron transfer distance at the same time complicates obtaining contact electron transfer rate constants from diffusion-electron transfer coupling data.

Another example of diffusion-electron transfer coupling was found recently in the self-diffusion of an undiluted molten salt Co(II) bipyridine-poly-ether derivative (Entries# 27,28). The self exchange rate constant for the Co(II/III) couple is very small, so oxidation of Co(II) measures the physical diffusivity D_{phys} (dis-regarding a small factor for its ionic migration). Reduction of the Co(II) complex produces, on the other hand, an apparent diffusivity D_{app} which is over 10^4-fold larger than D_{phys}. This is in sharp contrast to the $TCNQ^{-/0}$ example where, owing to the variation of electron transfer distance, D_{app} and D_{phys} are never very different. The difference in behavior of the $TCNQ^{-/0}$ and Co(II/I) couples arises because in the Co(II) bipyridine melt, the Co(II/I) D/A pair is undiluted by any solvent, and the reactants are always more or less in "contact", so the electron transfer distance is relatively constant. The electron transfer rate constant obtained for the melt phase Co(II/I) couple is $k_\delta = 2\times10^6\ M^{-1}s^{-1}$, much smaller than the rate constant for $[Co(bpy)_3]^{2+/1+}$ dissolved in acetonitrile.

The poly-ether tailed ferrocene Entry #10-13 and Figure 2 provide another example of diffusion-electron exchange coupling. The coupling in this example was originally interpreted[5] with the collision-rate limited Dahms-Ruff equation, which we now know is not appropriate. Re-examination of the data, assuming a literature value obtained in CH_3CN solution[20] for the ferrocene$^{0/+}$ k_{ex}, reveals that the $k_\delta\delta^2C/6$ term in Equation (19) is insignificant for all of the Figure 2 data at temperatures above the melting transition (the knee). Below that temperature, where physical diffusion of the ferrocene derivative is slower, electron self-change may contribute to the overall transport. However, considering the behavior of the TCNQ system and realizing that longer distance electron transfers may also occur in the ferrocene$^{0/+}$ couple, it is unlikely that the lower temperature D_{app} results in Figure 2 are in error by more than a factor of 2 or 3, at most.

ACKNOWLEDGEMENT. This research has been supported by grants from the National Science Foundation, the Department of Energy, and the Office of Naval Research.

REFERENCES

1. M. Watanabe, M. L. Longmire, and R. W. Murray, *J. Phys. Chem.*, **1990**, *94*, 2614.
2. H. Nishihara, F. Dalton, and R.W. Murray, *Anal. Chem.*, **1991**, *63*, 2955.
3. T. T. Wooster, M. L. Longmire, M. Watanabe, and R.W. Murray, *J. Phys. Chem.* **1991**, *95*, 5315.
4. T. T. Wooster, M. Watanabe, and R.W. Murray, *J. Phys. Chem.* **1992**, *96*, 5886.
5. M. Pinkerton, I. Le Mest, H. Zhang, M. Watanabe, R. W. Murray, *J. Amer. Chem. Soc.*, **1990**, *112*, 3730 (corr. pp 8317).
6. C. S. Velázquez, J. E. Hutchison, and R. W. Murray, *J. Amer. Chem. Soc.*, **1993**, *115*, 7896.
7. R. M. Wightman, *Science*, **1988**, *240*, 415.
8. (a) M. Armand, *Solid State Ionics*, **1983**, *9&10*, 745. (b) M. B. Armand, *Ann. Rev. Mater. Sci.*, 1986, *16*, 245. (c) C. A. Vincent, *Prog. Solid. State Chem.*, **1987**, *17*, 145. (d) M. A. Ratner, D. F. Shriver, *Chem. Rev.*, **1988**, *88*, 109. (e) M. B. Armand, J. M. Chabango, M. J. Duclot, *Fast Ion Transport in Solids*, J. Mundy, G. K. Shenoy, Pergamon: New York, 1979, p. 131. (f) M. Watanabe, N. Ogata, *Brit. Polym. J.*, **1988**, *20*, 181.
9. L. Geng, A. G. Ewing, J. C. Jernigan, and R. W. Murray, *Anal. Chem.*, **1986**, *58*, 852.
10. R. M. Wightman and D. O. Wipf, *Electroanalytical Chemistry*, A. J. Bard, Ed., Vol. 15, M. Dekker, NY, 1990.
11. A. J. Bard, L. Faulkner, *Electrochemical Methods: Fundamentals and Applications*; John Wiley & Sons, Inc., 1980.
12. O. Haas, unpublished results, Univ. No. Car. 1992.
13. M. L. Longmire, M. Watanabe, H. Zhang, T. T. Wooster, R. W. Murray, *Anal. Chem.*, **1990**, *62*, 747.
14. M. L. Longmire, M. Watanabe, H. Zhang, T. T. Wooster, R. W. Murray, *Anal. Chem.*, **1992**, *64*, 1132.
15. M. Poupart-Wilson, C. Velazquez, K. Hassett, Z. Porat, Univ. No. Car. Unpublished results, 1993.

16. (a) H. Dahms, H. *J. Phys. Chem.*, **1968**, *72*, 362. (b) I. Ruff, V. J. Friedrich, *ibid*, **1971**, *75*, 3297. (c) I. Ruff, V. J. Friedrich, K. Demeter, K. Csaillag. *ibid*, **1971**, *75*, 3303. (c) I. Ruff, I. Korosi-Odor, *Inorg. Chem.*, **1970**, *9*, 186. (d) I. Ruff, *Electrochim. Acta*, **1970**, *15*, 1059.

17. R. W. Murray, Ed., **Molecular Design of Electrode Surfaces**, in "Techniques of Chemistry" J. Wiley and Sons, NY, 1992.

18. D. A. Buttry, F. C. Anson, *J. Am. Chem. Soc.*, **1983**, *105*, 685.

19. R. A. Marcus, N. Sutin, *Biochim. et Biophys. Acta*, **1985**, *811*, 265.

20. R. M. Nielson, G. E. McManis, L. K. Sanford, M. J. Weaver, *J. Phys. Chem.* **1989**, *93*, 2152.

Table I. RELATIONS FOR INCOMPENSATED RESISTANCE AND FOR LINEAR AND RADIAL DIFFUSION CURRENTS AT MICRODISK AND MICROBAND ELECTRODES[a]

	Linear[b]		Radial[c]	
Disk Current	$2.69\times10^{5}n^{\frac{3}{2}}D^{\frac{1}{2}}v^{\frac{1}{2}}C(\pi r^{2})$	(1)	$4nFrDC$	(2)
Band Current	$2.69\times10^{5}n^{\frac{3}{2}}D^{\frac{1}{2}}v^{\frac{1}{2}}C(wL)$	(3)	$\frac{\pi nFDCL}{\ln\left[\frac{8(Dt)^{\frac{1}{2}}}{w}\right]}$	(4)
$\frac{i_{DISK}}{i_{BAND}}$	$\frac{\pi r^{2}}{wL}$	(5)	$\left(\frac{4r}{\pi L}\right)\ln\left[\frac{8(Dt)^{\frac{1}{2}}}{w}\right]$	(6)
Disk Resistance	$\frac{\rho}{4r}$	(7)	$\frac{\rho}{4r}$	(8)
Band Resistance	$\left(\frac{\rho}{\pi L}\right)\ln\left(\frac{2d}{w}\right)$	(9)	$\left(\frac{\rho}{\pi L}\right)\ln\left(\frac{2d}{w}\right)$	(10)
$\frac{R_{DISK}}{R_{BAND}}$	$\frac{\pi L}{4r\ln\left(\frac{2d}{w}\right)}$	(11)	$\frac{\pi L}{4r\ln\left(\frac{2d}{w}\right)}$	(12)
$i_{DISK}R_{DISK}$	$2.69\times10^{5}n^{\frac{3}{2}}D^{\frac{1}{2}}v^{\frac{1}{2}}C\pi\rho r$	(13)	$\rho nFDC$	(14)
$i_{BAND}R_{BAND}$	$2.69\times10^{5}n^{\frac{3}{2}}D^{\frac{1}{2}}v^{\frac{1}{2}}C\pi^{-1}\rho w\ln\left(\frac{2d}{w}\right)$	(15)	$\frac{\rho nFDC\ln\left(\frac{2d}{w}\right)}{\ln\left[\frac{8(Dt)^{\frac{1}{2}}}{w}\right]}$	(16)
$\frac{i_{DISK}R_{DISK}}{i_{BAND}R_{BAND}}$	$\frac{\pi^{2}r}{w\ln\left(\frac{2d}{w}\right)}$	(17)	$\frac{\ln\left[\frac{8(Dt)^{\frac{1}{2}}}{w}\right]}{\ln\left(\frac{2d}{w}\right)}$	(18)

[a]In the equations, n is number of electrons, D is diffusion coefficient (more appropriately called D_{app}), C is concentration, v is potential sweep rate, r is microdisk radius, L and w are microband length and width respectively, δ is specific solution ionic resistance, and d is distance between working and reference electrode.
[b]For peak current in potential sweeps.
[c]Plateau currrents. In the case of microbands the currents are limiting values for potential steps.

TABLE II. SELECTED DIFFUSION COEFFICIENT DATA FOR REDOX PROBES IN POLY-ETHER SOLVENTS[1-6,13,14]

ENTRY No.	DIFFUSING PROBE (CONC., M)	MICROELECTR.	POLYMER SOLVENT (O/Li)	TEMP.	D (cm^2/s)
1	$CpFeCO_2H$	r = 12.5μm	Network-PEO (50)	65°C	2.8×10^{-7}
2	$CpFeCpCO_2^-$	r = 12.5μm	Network-PEO (50)	65°C	7.4×10^{-8}
3	$CpFeCpCH_2N(CH_3)_3^+$	r = 12.5μm	Network-PEO (50)	65°C	7.5×10^{-8}
4	Cp_2^*Fe	r = 12.5μm	Network-PEO (50)	65°C	2.2×10^{-8}
5	Cp_2Fe (0.05M), $Cp_2Fe^+(ClO_4)^-$ (0.05M)	IDA	MPEG-400 (16)	23°C	2.6×10^{-8}
6	Cp_2Fe (0.2M), $Cp_2Fe^+(ClO_4)^-$ (0.2M)	IDA	MPEG-400 (16)	23°C	1.5×10^{-8}
7	Cp_2Fe (0.1M), $Cp_2Fe^+(ClO_4)^-$ (0.1M)	IDA	MPEG-1000 (16)	23°C	6.2×10^{-10}
8	Cp_2Fe (0.4M), $Cp_2Fe^+(ClO_4)^-$ (0.4M)	IDA	MPEG-1000 (16)	23°C	1.6×10^{-9}
9	$CpFeCpCO_2H$ (53mM)	r = 5μm	MPEG-2000 (16)	65°C	2.2×10^{-7}
10	CpFeCpCONH-MPEG-2000 (0.042M)	r = 5μm	MPEG-2000 (16)	65°C	1.8×10^{-8}
11	CpFeCpCONH-MPEG-2000 (0.43M)	r = 5μm	NONE (16)	65°C	1.8×10^{-8}
12	CpFeCpCONH-MPEG-2000 (0.43M)	r = 5μm	NONE (16)	23°C	4×10^{-12}
13	$[Co(bpy)_3]^{2+/3+}$	r = 5μm	Network-PEO (50)	65°C	4×10^{-8}
14	$[Co(bpy)_3]^{2+/3+}$	r = 5μm	MPEG-400 (16)	66°C	2.4×10^{-7}
15	$[Co(bpy)_3]^{2+/3+}$	r = 5μm	MPEG-1000 (16)	65°C	1.8×10^{-7}
16	$[Os(phen)_3]^{2+/3+}$	r = 5μm	PEO-600,000 (16) ($LiPF_3SO_3$)	65°C	1.4×10^{-7}
17	$[Os(phen)_3]^{2+/3+}$	r = 5μm	PEO-600,000 (16) ($LiPF_3SO_3$)	25°C	1.6×10^{-10} (0.35wt% sorbed CH_3CN)
18	$[Os(phen)_3]^{2+/3+}$	r = 5μm	PEO-600,000 (16) ($LiPF_3SO_3$)	25°C	2.1×10^{-8} (10 wt% sorbed CH_3CN)

TABLE II CONTINUED. . .

ENTRY No.	DIFFUSING PROBE (CONC., M)	MICROELECTR.	POLYMER SOLVENT (O/Li)	TEMP	D (cm^2/s)
19	$TCNQ^{1-/2-}$ (75mM) $TCNQ^{1-/0}$ $k_s\delta^2=1.2\times10^{-7}$ $M^{-1}s^{-1}$	r = 12.5μm	NETWORK-PEO (50)	23°C	1.35×10^{-9} 2.87×10^{-9}
20	$TCNQ^{1-/2-}$ (75mM) $TCNQ^{1-/0}$ $k_s\delta^2=3.4\times10^{-6}$ $M^{-1}s^{-1}$	r = 12.5μm	NETWORK-PEO (50)	66°C	2.19×10^{-8} 6.42×10^{-8}
21	$TCNQ^{1-/2-}$ (75mM) $TCNQ^{1-/0}$ $k_s\delta^2=5.7\times10^{-8}$ $M^{-1}s^{-1}$	r = 12.5μm	NETWORK-PEO (20)	22°C	3.67×10^{-10} 1.08×10^{-9}
22	$TCNQ^{1-/2-}$ (75mM) $TCNQ^{1-/0}$ $k_s\delta^2=2.2\times10^{-6}$ $M^{-1}s^{-1}$	r = 12.5μm	NETWORK-PEO (20)	66°C	1.53×10^{-8} 4.22×10^{-8}
23	$TCNQ^{1-/2-}$ (75mM) $TCNQ^{1-/0}$ $k_s\delta^2=2.8\times10^{-10}$ $M^{-1}s^{-1}$	r = 12.5μm	NETWORK-PEO (13)	22°C	5.57×10^{-11} 5.92×10^{-11}
24	$TCNQ^{1-/2-}$ (75mM) $TCNQ^{1-/0}$ $k_s\delta^2=1.1\times10^{-8}$ $M^{-1}s^{-1}$	r = 12.5μm	NETWORK-PEO (13)	66°C	6.28×10^{-9} 6.42×10^{-9}
25	$TCNQ^{1-/2-}$ (75mM) $TCNQ^{1-/0}$ $k_s\delta^2=7.9\times10^{-11}$ $M^{-1}s^{-1}$	r = 12.5μm	NETWORK-PEO (10)	22°C	5.55×10^{-12} 6.54×10^{-12}
26	$TCNQ^{1-/2-}$ (75mM) $TCNQ^{1-/0}$ $k_s\delta^2=1.6\times10^{-8}$ $M^{-1}s^{-1}$	r = 12.5μm	NETWORK-PEO (10)	66°C	5.45×10^{-10} 7.43×10^{-10}
27	$[Co(bpy(eeem)_2)_3]^{2+/3+}$	r = 5μm	None (None)	23°C	3×10^{-13}
28	$[Co(bpy(eeem)_2)_3]^{2+/1+}$	r = 5μm	None (None)	23°C	6×10^{-9}

Figure Captions

Figure 1. (A) Near radial diffusion of a 5 m<u>M</u> solution of the ferrocene carboxylic ester poly-ethylene oxide derivative $CpFeCpCO_2(CH_2CH_2O)_{43}CH_3$ (Fc2000) in linear poly-ethylene oxide of MW 20,000 containing $LiClO_4$ at O/Li = 16; microdisk radius 5 μm, 70°C, 1 mV/s, D = $1.1x10^{-8}$ cm^2/s. (B) Oxidation and reduction waves for 10 m<u>M</u> LiTCNQ dissolved in network PEO, at indicated temperatures, 20 mV/s, 12.5 μm radius microdisk. $D_{1/0}$ = $6.7x10^{-9}$, $3.4x10^{-7}$ cm^2/s at 23,101°C, respectively. $D_{1/2}$ = $5.4x10^{-9}$, $3.0x10^{-7}$ cm^2/s at 23,101°C respectively. Adapted fro 4. (C) Mixed, linear-radial diffusion for oxidation of 0.43<u>M</u> ferrocene sites in the undiluted ferrocene carboxylic amide poly-ethylene oxide derivative $CpFeCpCONH(CH_2CH_2O)_{43}CH_3$ (FcMPEG) containing $LiClO_4$ at O/Li = 16; microdisk radius 5 μm, 62°C, 5 mV/s, D = $1.5x10^{-8}$ cm^2/s. Adapted from Ref. 5.

Figure 2. Dependence of D_{app} on temperature for 5 mM $CpFeCpCO_2H$ in linear methyl end-capped PEO of nominal MW 2000 (MPEG-2000, circles) and for undiluted $CpFeCpCONH(CH_2CH_2O)_{43}CH_3$ (FcMPEG) (triangles), with (O/Li = 16:1) $LiClO_4$ electrolyte, microdisk of radius 5 μm. Filled circles for chronoamperometric measurements; open circles were radial diffusion. The inset shows enlarged plots for data above T_M and an additional plot (middle line) for 43 mM FcMPEG in MPEG-2000; E_A for diffusion is 8.7, 7.8, 8.7 kcal/mol, top to bottom.

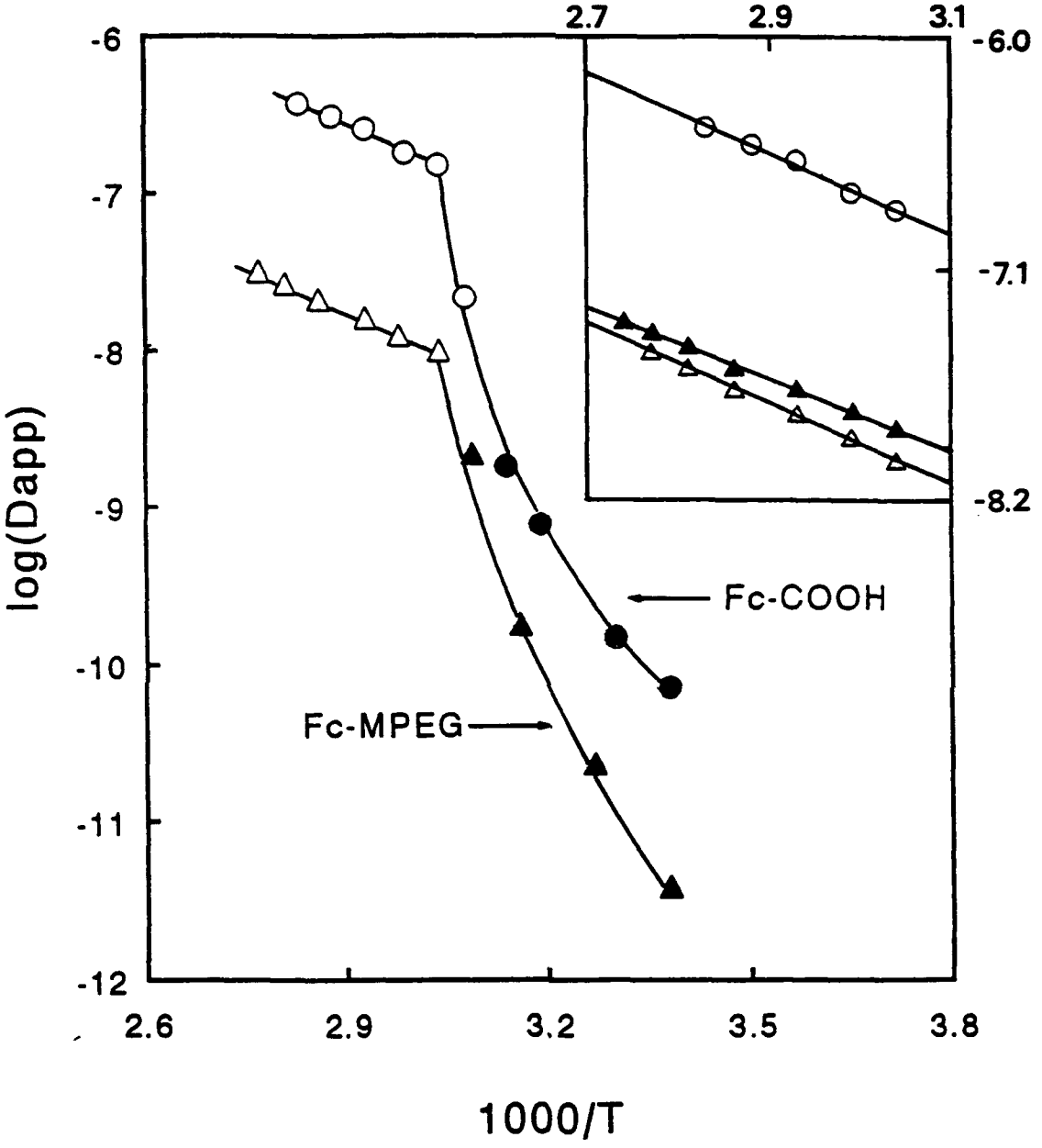
2.7
2.9
3.1
-6
-7
-8
-9
-10
-11
-12
-6.0
-7.1
-8.2
log(Dapp)
Fc-COOH
Fc-MPEG
2.6
2.9
3.2
3.5
3.8
1000/T

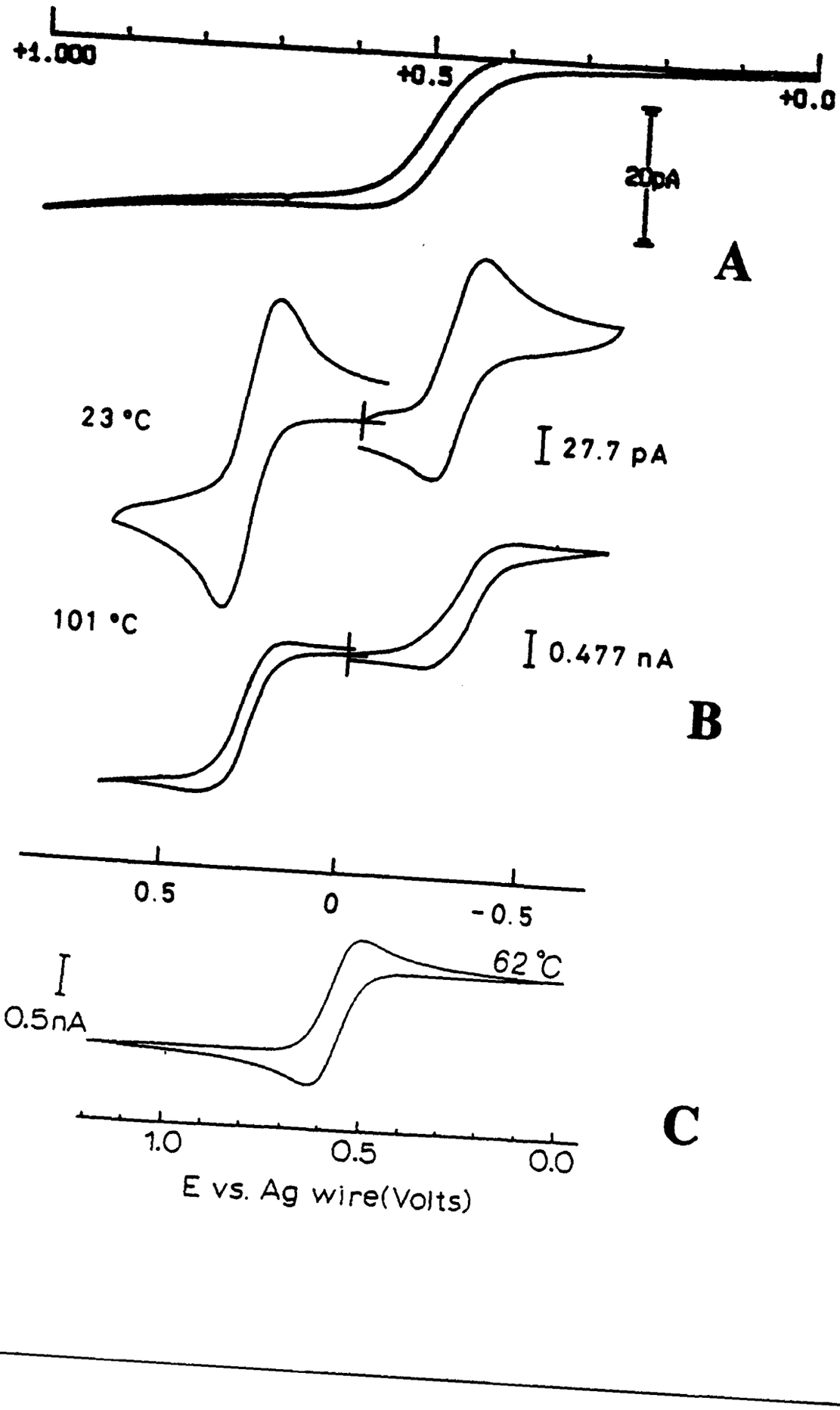
+1.000
+0.5
+0.0
20pA
A
23 °C
I 27.7 pA
101 °C
I 0.477 nA
B
0.5
0
-0.5
I
0.5nA
62 °C
1.0
0.5
0.0
C
E vs. Ag wire(Volts)